HHS Public Access

Author manuscript

Mol Imaging Biol. Author manuscript; available in PMC 2018 April 17.

Published in final edited form as:

Mol Imaging Biol. 2018 April ; 20(2): 200–204. doi:10.1007/s11307-017-1113-7.

Translocator Protein PET Imaging in a Preclinical Prostate Cancer Model

Mohammed N. Tantawy[1,2], **H. Charles Manning**[1,2,3,4], **Todd E. Peterson**[1,2], **Daniel C. Colvin**[1], **John C. Gore**[1,2], **Wenfu Lu**[5], **Zhenbang Chen**[5], and **C. Chad Quarles**[6]

[1]Vanderbilt University Institute of Imaging Science (VUIIS), Vanderbilt University Medical Center, 1161 21st Ave. S., AA 1105 MCN, Nashville, TN, 37232, USA

[2]Department of Radiology and Radiological Sciences, Vanderbilt University Medical Center, Nashville, TN, 37232, USA

[3]Vanderbilt-Ingram Cancer Center, Vanderbilt University Medical Center, Nashville, TN, 37232, USA

[4]Program in Chemical and Physical Biology, Vanderbilt University Medical Center, Nashville, TN, 37232, USA

[5]Department of Biochemistry and Cancer Biology, Meharry Medical College, Nashville, TN, 37208, USA

[6]Imaging Research, Barrow Neurological Institute, 350 W Thomas Rd, Phoenix, AZ, 85013, USA

Abstract

Purpose—The identification and targeting of biomarkers specific to prostate cancer (PCa) could improve its detection. Given the high expression of translocator protein (TSPO) in PCa, we investigated the use of [^{18}F]VUIIS1008 (a novel TSPO-targeting radioligand) coupled with positron emission tomography (PET) to identify PCa in mice and to characterize their TSPO uptake.

Procedures—Pten$^{pc-/-}$, Trp53$^{pc-/-}$ prostate cancer-bearing mice (n = 9, 4–6 months old) were imaged in a 7T MRI scanner for lesion localization. Within 24 h, the mice were imaged using a microPET scanner for 60 min in dynamic mode following a retro-orbital injection of ~ 18 MBq [^{18}F]VUIIS1008. Following imaging, tumors were harvested and stained with a TSPO antibody. Regions of interest (ROIs) were drawn around the tumor and muscle (hind limb) in the PET images. Time-activity curves (TACs) were recorded over the duration of the scan for each ROI. The mean activity concentrations between 40 and 60 min post radiotracer administration between tumor and muscle were compared.

Results—Tumor presence was confirmed by visual inspection of the MR images. The uptake of [^{18}F]VUIIS1008 in the tumors was significantly higher ($p < 0.05$) than that in the muscle, where

Correspondence to: C. Chad Quarles; chad.quarles@barrowneuro.org.

Compliance with Ethical Standards

Conflict of Interest

The authors declare that they have no conflict of interest.

the percent injected dose per unit volume for tumor was 7.1 ± 1.6 % ID/ml and that of muscle was < 1 % ID/ml. In addition, positive TSPO expression was observed in tumor tissue analysis.

Conclusions—The foregoing preliminary data suggest that TSPO may be a useful biomarker of PCa. Therefore, using TSPO-targeting PET ligands, such as [^{18}F]VUIIS1008, may improve PCa detectability and characterization.

Keywords

Translocator protein; Prostate cancer; PET

Introduction

Prostate cancer (PCa) is one of the most common malignancies in the world and the sixth leading cause of cancer-related fatalities among men [1]. In the USA, it is the second most fatal cancer in men after lung cancer despite the availability of a variety of screening and diagnostic tools. There is a need for improved imaging technology and/or the use of suitable molecular imaging agents that target specific biomarkers of this cancer.

Positron imaging tomography (PET) with 2-deoxy-2-[^{18}F]fluoro-D-glucose ([^{18}F]FDG) has been used to detect PCa [2], but due to low sensitivity and overlap with prostatitis, prostatic hypertrophy, and radiotracer renal secretion and accumulation in the bladder, new PET radiotracers are highly desired [3]. Choline PET imaging, using [^{11}C]choline or [^{18}F]fluoroethylcholine, is more sensitive for detecting PCa than [^{18}F]FDG [4–7]. However, the accuracy of this method requires the administration of higher radiotracer activities and delayed imaging (for the F-18 labeled ligands) [4], may be confounded by false positives due to non-specific inflammation-associated uptake [8], and requires an on-site cyclotron in the case of [^{11}C]choline. Accordingly, there remains a clinical interest in identifying more sensitive and specific molecular imaging agents that improve PCa detection.

Translocator protein (TSPO), typically located in the outer mitochondrial membrane, is mainly responsible for transporting cholesterol across the membrane for cell signaling and steroid biosynthesis [9, 10]. TSPO had been found to be overly expressed and even involved in the progression of many cancers including PCa [11, 12]. Furthermore, TSPO has been used as a target for PCa therapy using PK11195 and lorazepam [11]. Recently, we developed [^{18}F]VUIIS1008 for TSPO PET imaging of cancer and demonstrated that it reliably targets TSPO in glioma [13]. [^{18}F]VUIIS1008 exhibits higher binding affinity compared with its parent ligand, [^{18}F]DPA-714, and offers improved imaging qualities for cancer imaging [13].

In this work, we investigate [^{18}F]VUIIS1008 PET imaging for detecting primary prostate tumors *via* targeting TSPO receptors within the tumor in mouse models of PCa.

Materials and Methods

All studies involving small animals were conducted in accordance with federal and institutional guidelines and approved by Vanderbilt's Institutional Animal Care and Use Committee.

Animal Models

Imaging data was acquired in the genetically engineered *Pten/Trp53* conditional mouse model ($Pten^{pc\ -/-}$; $Trp53^{pc\ -/-}$) of PCa. This model recapitulates PCa progression in human cancers, including the development of castration-resistant PCa [14, 15]. Imaging studies were initiated following the spontaneous development (4–6 months old) of PCa in the mice ($n = 9$). The mice weighed 33 ± 3 g (mean ± SD).

MRI

Prior to scanning, mice were anesthetized, using inhalation of 2 % isoflurane mixed with 98 % oxygen, secured in a rodent imaging frame and placed in a 38-mm inner diameter radiofrequency (RF) coil. MRI data was acquired using a Varian 7T imaging system (Varian Inc., Palo Alto, CA). During the imaging examination, a constant body temperature of 37 °C was maintained using heated air flow.

Multi-slice scout images were acquired using a gradient echo sequence with the following parameters: field of view (FOV) = 50 × 50 mm, data matrix = 128 × 128, slice thickness = 2 mm, flip angle = 35°, repetition time (TR) = 75 ms, echo time (TE) = 5 ms, and number of acquisitions = 4. Following scout imaging, T2-weighted fast-spin echo images were acquired of 32 slices in the axial and sagittal planes, with field of view (FOV) = 33 × 33 mm, slice thickness = 1.0 mm, and data matrix = 256 × 256. Additional parameters included repetition time (TR) = 2.75 s, effective echo time (TE) = 36 ms, echo train length = 8, echo spacing = 9 ms, and number of acquisitions (NEX) = 12. A pneumatic pillow was used to monitor the respiration cycle of the mice, as well as trigger the imaging acquisition to collect data at the same time point in the respiration cycle to reduce motion-induced imaging artifacts.

PET/CT

PET and CT data of each animal was acquired within 24 h of the MR scans. The mice were anesthetized with 2 % isoflurane and positioned in a microPET Focus 220 (Siemens, Knoxville, TN). Dynamic PET data was acquired for 60 min following a retro-orbital administration of ~ 18 MBq/0.2 ml [^{18}F]VUIIS1008. The dynamic data were binned into the following variable length frames: twelve 5-s frames, four 60-s frames, one 5-min frame, and five 10-min frames. The MAP algorithm was used to reconstruct the data into 128 × 128 × 95 slices with a voxel size of 0.095 × 0.095 × 0.08 cm^3 at a beta value of 0.01. CT scans were next acquired to facilitate anatomic co-registration of the PET and MRI data. Mice were imaged in an Inveon CT (Siemens preclinical, Knoxville TN) following an IP injection of ~ 0.2 ml of the contrast agent Optiray (Mallinckrodt Inc., St. Louis, MO), which enables visualization of the bladder. Note that TSPO ligands are not cleared *via* the kidneys [13]. The CT data was collected using the following parameters: beam intensity = 180 mAs, tube voltage = 80 kVp, reconstructed image matrix = 512 × 512 × 512, and voxel size = 0.1 × 0.1 × 0.1 mm^3.

Analysis

Amide (amide.sourceforge.net) was used to co-register the CT, MRI, and PET images. The MRI images were used to define three dimensional regions of interest (ROIs) encompassing

the tumors in the abdominal area and muscle on the hind limb. Time-activity curves (TACs) within each ROI were computed as the radiotracer concentration normalized to the administered activity. The late radiotracer uptake, computed as the mean concentration between 40 and 60 min post-injection, in tumor and muscle ROIs were also compared using a paired *t* test, with a significance threshold of $p < 0.05$. Statistical analysis was completed with the GraphPad Prism software (v.6.01).

Histology

Upon completion of the PET/CT scans, the mice were euthanized and the tumors were harvested fixed in 4 % buffered formalin for 48 h, followed by paraffin embedding for histology and immunohistochemistry (IHC). Tissue sections (5.0 μm) were then stained with TSPO-specific rabbit polyclonal anti-rat/anti-mouse antibody (Novus Biologicals, LLC, Littleton, CO). Immunoreactivity was assessed using a horseradish peroxidase detection kit (Dako, Glostrup, DK). Sequential tissue sections were also stained with H&E and Ki-67 (for proliferation). The sections were then imaged using bright-field microscopy (Leica Microsystems, Inc., Buffalo Grove, IL, USA).

Results

Serial imaging with MRI was used to first visualize the development of tumors as shown in Fig. 1. Tumors exhibited high uptake of [^{18}F]VUIIS1008, with little to no uptake observed in the muscle (Fig. 2). Upon harvesting the tumors, we found them to be greater than 2 cm^3 in size and filled most of the abdominal area which correlates with the MR images. Presence of cells confirmed *via* H&E and positive staining for proliferation *via* Ki 67 denote that the majority of tumor was active and not necrotic. Tumors that exhibited high [^{18}F]VUIIS1008 uptake were histologically confirmed to have TSPO expression. As shown in Fig. 3, the uptake of [^{18}F]VUIIS1008 in the tumor appeared reached equilibrium approximately 25 min post-injection. Across all animals, the concentration of [^{18}F]VUIIS1008 in the tumor (7.1 ± 1.6 % ID/ml) was significantly higher ($p < 0.05$) than that found in muscle (0.7 ± 0.2 % ID/ml) (Fig. 4).

Discussion

In the context of cancer, elevated TSPO expression has been associated with enhanced progression, reduced survival, and metastatic potential [10, 13]. It has been implicated in numerous cancer types, including breast, colon, brain, and other cancers [10, 13, 16, 17]. Expanding upon our previous studies in glioma [13], we now provide evidence that the TSPO radioligand, [^{18}F]VUIIS1008, can be used to detect primary prostate tumors. TSPO expression in the tumors of *Pten*/*Trp53* mice was regionally heterogeneous, confirmed with immunohistochemistry, but was consistently observed across tumors, as determined using [^{18}F]VUIIS1008.

Prior *in vivo* studies have shown that [^{18}F]VUIIS1008 exhibits exceptional binding potential and, correspondingly, promising tumor-to-background ratios. Extending these observations to PCa, [^{18}F]VUIIS1008 exhibited very low washout rates with near constant %ID/ml between 5 and 60 min after administration. If this is recapitulated in human PCa, this would

be a valuable clinical characteristic since it would enable static imaging at a specific time point after injection. Immunohistochemical analysis of PCa tissue microarrays revealed that, as compared to normal tissue and benign lesions, TSPO expression is significantly higher in primary PCa, prostatic intraepithelial neoplasia, and PCa metastasis [11]. Accordingly, it is reasonable to expect significant differences in the uptake of [^{18}F]VUIIS1008 between PCa and normal tissue, which would enable regional localization of PCa burden. Another clinical advantage of [^{18}F]VUIIS1008 is its clearance *via* the liver as opposed to the bladder, where tracer retention could confound the regional detection of PCa.

Conclusions

In conclusion, this study demonstrates the feasibility of using [^{18}F]VUIIS1008 to evaluate TSPO expression in PCa. The high tumor uptake of [^{18}F]VUIIS1008 observed in the *Pten*/*Trp53* mice implicates its potential use for detecting the development of castration-resistant PCa and metastatic spread.

Acknowledgments

This work was supported by DOD W81XWH-12-1-0245 and R01 CA163806. The microPET Focus 220 was funded by NIH 1S10 RR017858, and the Inveon microPET/CT was funded by NIH 1S10 OD016245.

References

1. Jain S, Saxena S, Kumar A. Epidemiology of prostate cancer in India. Meta Gene. 2014; 2:596–605. [PubMed: 25606442]
2. Liu Y. Diagnostic role of fluorodeoxyglucose positron emission tomography-computed tomography in prostate cancer. Oncol Lett. 2014; 7:2013–2018. [PubMed: 24932281]
3. Cho SY, Szabo Z. Molecular imaging of urogenital diseases. Sem Nucl Med. 2014; 44:93–109.
4. Chan J, Syndikus I, Mahmood S, et al. Is choline PET useful for identifying intraprostatic tumour lesions? A literature review. Nucl Med Comm. 2015; 36:871–880.
5. Vagnoni V, Brunocilla E, Bianchi L, et al. State of the PET/CT with 11-choline and 18F-fluorocholine in the diagnosis and follow-up of localized and locally advanced prostate cancer. Arch Espan Urol. 2015; 68:354–370. [PubMed: 25948806]
6. Vorster M, Modiselle M, Ebenhan T, et al. Fluorine-18-fluoroethylcholine PET/CT in the detection of prostate cancer: a South African experience. Hell J Nucl Med. 2015; 18:53–59. [PubMed: 25840573]
7. Giovacchini G, Picchio M, Coradeschi E, et al. [^{11}C]choline uptake with PET/CT for the initial diagnosis of prostate cancer: relation to PSA levels, tumour stage and anti-androgenic therapy. Eur J Nucl Med Mol Imaging. 2008; 35:1065–1073. [PubMed: 18200444]
8. Garcia Vicente AM, Nunez Garcia A, Soriano Castrejon AM, et al. Pitfalls with ^{18}F-choline PET/CT in patients with prostate cancer. Revista Esp Med Nucl Imagen Mol. 2013; 32:37–39.
9. Rone MB, Fan J, Papadopoulos V. Cholesterol transport in steroid biosynthesis: role of protein-protein interactions and implications in disease states. Biochim Biophys Acta. 2009; 1791:646–658. [PubMed: 19286473]
10. Buck JR, McKinley ET, Hight MR, et al. Quantitative, preclinical PET of translocator protein expression in glioma using ^{18}F-N-fluoroacetyl-N-(2,5-dimethoxybenzyl)-2-phenoxyaniline. J Nucl Med. 2011; 52:107–114. [PubMed: 21149488]
11. Fafalios A, Akhavan A, Parwani AV, Bies RR, McHugh KJ, Pflug BR. Translocator protein blockade reduces prostate tumor growth. Clin Cancer Res. 2009; 15:6177–6184. [PubMed: 19789311]

12. Batra S, Alenfall J. Characterization of peripheral benzodiazepine receptors in rat prostatic adenocarcinoma. Prostate. 1994; 24:269–278. [PubMed: 8170839]
13. Tang D, Nickels ML, Tantawy MN, et al. Preclinical imaging evaluation of novel TSPO-PET ligand 2-(5,7-Diethyl-2-(4-(2-[^{18}F]fluoroethoxy)phenyl)pyrazolo[1,5-a]pyrimidin-3-yl)- N,N-diethylacetamide ([^{18}F]VUIIS1008) in glioma. Mol Imaging Biol. 2014; 16:813–820. [PubMed: 24845529]
14. Chen Z, Trotman LC, Shaffer D, et al. Crucial role of p53-dependent cellular senescence in suppression of Pten-deficient tumorigenesis. Nature. 2005; 436:725–730. [PubMed: 16079851]
15. Lu W, Liu S, Li B, et al. SKP2 inactivation suppresses prostate tumorigenesis by mediating JARID1B ubiquitination. Oncotarget. 2015; 6:771–788. [PubMed: 25596733]
16. Sexton M, Woodruff G, Cudaback E, et al. Binding of NIR-conPK and NIR-6T to astrocytomas and microglial cells: evidence for a protein related to TSPO. PLoS One. 2009; 4:e8271. [PubMed: 20020060]
17. Wyatt SK, Manning HC, Bai M, et al. Preclinical molecular imaging of the translocator protein (TSPO) in a metastases model based on breast cancer xenografts propagated in the murine brain. Curr Mol Med. 2012; 12:458–466. [PubMed: 22348613]

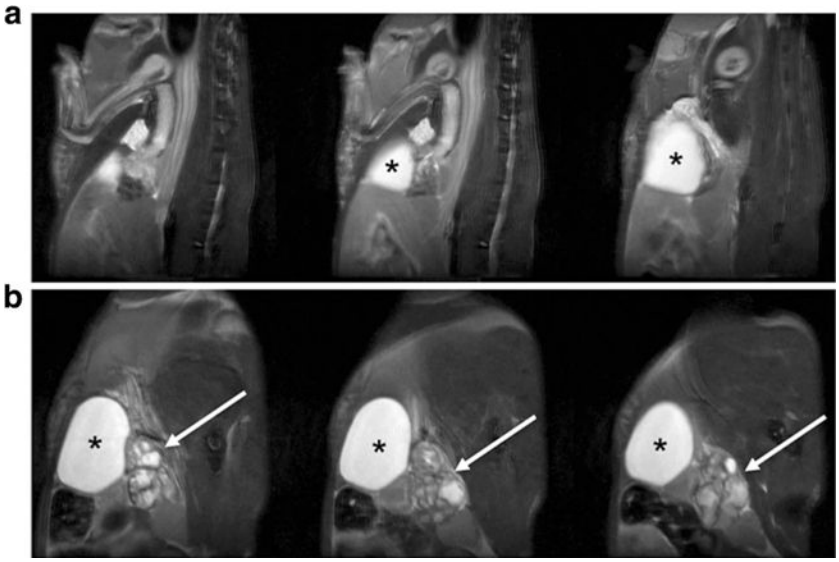

Fig. 1.

Representative multi-slice T2-weighed MR images of **a** wild-type control and **b** Pten/Trp53 mutant mouse with prostate cancer, illustrating locations of enlarged prostate tumor (arrow) and bladder (asterisk).

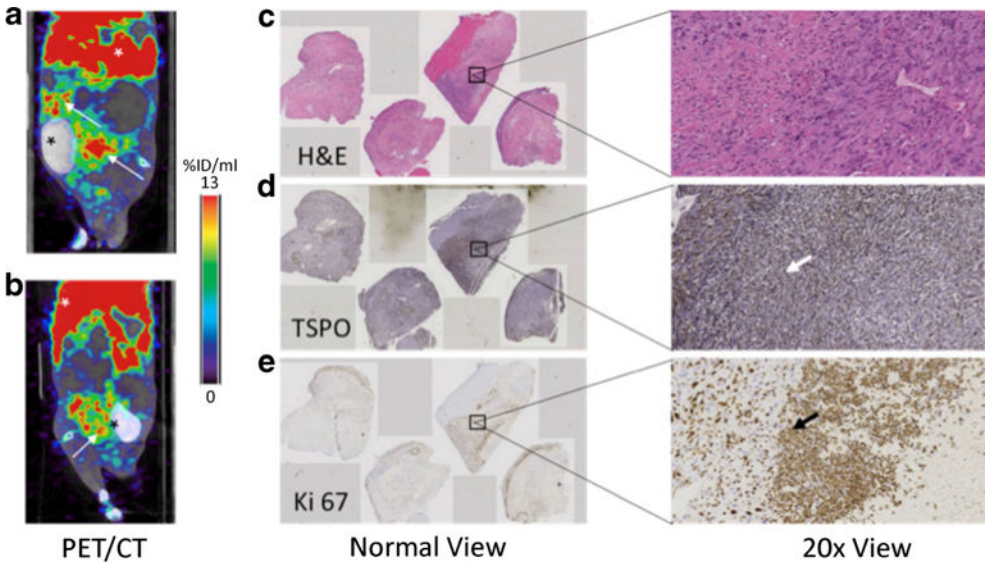

Fig. 2.

a Coronal and **b** sagittal PET/CT images of a prostate cancer-bearing mouse injected with [^{18}F]VUIIS1008. The PET images were summed between 40 and 60 min post radiotracer administration. Mice were injected with CT contrast agent Optiray. White arrows in the PET/CT images denote location of tumors (confirmed via gross examination) and the liver, respectively. Black asterisks denote bladder which contains the CT contrast agent. **c**, **d**, **e** Immunohistochemical analysis of adjacent sections confirm tumor cells via H&E, high density of TSPO expression (brown), and active cellular proliferation via Ki-67 staining (brown), respectively, at normal and 20 times magnification. The arrows in each stained image point to a positive stain as an example.

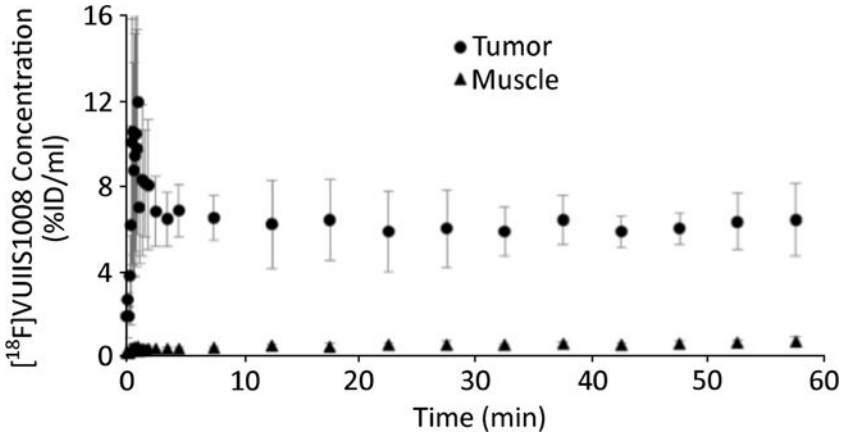

Fig. 3.

Average time-activity curves of [^{18}F]VUIIS1008 in tumor and muscle regions of interest. The error bars illustrate the standard deviation at each time point across animals (n = 9). Tumor uptake was markedly highly than that found in muscle and essentially constant between 5 and 60 min after administration.

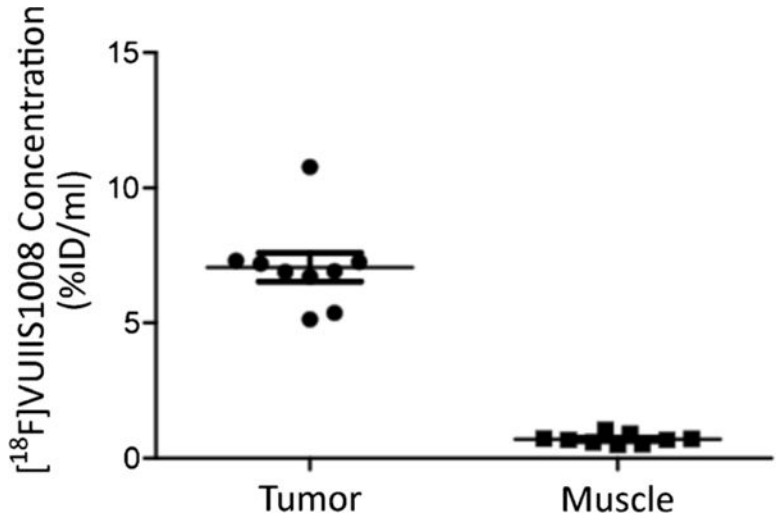

Fig. 4.

Comparison of [^{18}F]VUIIS1008 uptake, summed between 40 and 60 min post radiotracer administration, in tumor and muscle regions of interest. The tumor uptake was ten times higher than that found in muscle.